Journal of Alloys and Compounds 670 (2016) 85–95

Contents lists available at ScienceDirect

Journal of Alloys and Compounds

journal homepage: http://www.elsevier.com/locate/jalcom

Densification, characterization and oxidation studies of novel TiB_2+EuB_6 compounds

T.S.R.Ch. Murthy [a, *], J.K. Sonber [a], B. Vishwanadh [a], A. Nagaraj [b], K. Sairam [a], R.D. Bedse [a], J.K. Chakravartty [a]

[a] Materials Group, Bhabha Atomic Research Centre, Mumbai, India
[b] Laser and Plasma Technology Division, Bhabha Atomic Research Centre, Mumbai, India

ARTICLE INFO

Article history:
Received 8 December 2015
Received in revised form
14 January 2016
Accepted 27 January 2016
Available online 30 January 2016

Keywords:
TiB_2
EuB_6
Hot-pressing
Hardness
Fracture toughness
Elastic modulus
Oxidation studies

ABSTRACT

TiB_2+EuB_6 ceramic samples with different EuB_6 contents were fabricated using hot -pressing technique. The introduction of EuB_6 promoted the sinterability, fracture toughness and oxidation resistance of TiB_2. 98.7% TD achieved by adding 2.5% EuB_6 to TiB_2 by hot pressing at a relatively low temperature of 1750 °C, 35 MPa, 1h. Formation of complete solid solution of TiB_2+EuB_6 observed for all the samples by XRD, EDS and EBSD. Hardness of all samples is measured in the range of 24–27 GPa ~50% higher fracture toughness value of 5.2 MPa $m^{1/2}$ was obtained in the 2.5% EuB_6 contained sample compared to monolithic TiB_2. Enhancement of oxidation resistance of TiB_2 was observed by EuB_6 addition due to the formation of $EuBO_3$ and Eu_2O_3. Oxidized cross section of TiB_2+EuB_6 sample was measured as 340 μm, which is ~35% less than that of monolithic TiB_2 (520 μm), after oxidation at 1400 °C for 8h.

1. Introduction

Titanium diboride (TiB_2) is an increasingly important ceramic material for engineering applications, owing to the excellent combination of physicochemical and thermo-mechanical properties such as high melting temperature, high thermal conductivity, extreme hardness, high young's modulus, low thermal expansion coefficient, low density [1,2]. These properties make it ideal for use as cutting tools, wear resistance materials, coating materials, metal melting crucibles, impact resistant armors and electrodes [1–3]. TiB_2 is also a candidate material for neutron absorber in nuclear reactors owing to the presence of boron [1–4]. However, TiB_2 is rather limited in real applications due to problems associated with their consolidation and poor fracture toughness. High melting point, low self-diffusion coefficient and contamination with oxide layers on the surface of particles make it difficult to densification [1–5]. These setbacks have provided the driver for considerable research efforts to improve both the sinterability and toughness. One route employed to improve the sinterability/toughness of TiB_2 is to add a suitable sinter additive, such that it lowers the sintering temperature and improves the fracture toughness [1,6].

A significant research activity has been reported to use several sinter additives and studied the effect of sinter additive on mechanical/physical properties of monolithic TiB_2 [1–7]. In particular, an extensive and critical literature analysis has been reported on the role of metallic binders (e.g. Ni, Fe, Cu, Co, Ti) in the densification of TiB_2. More than 99% TD was achieved by liquid phase sintering [1,7,8]. However, the presence of metallic binder is not desirable for high temperature structural applications. Therefore, studies related to the use of non-metallic sinter-additives have also been pursued. Several ceramic additives such as AlN, $MoSi_2$, $CrSi_2$, WSi_2, $TiSi_2$, SiC, Si_3N_4, CrB_2, B_4C, TaC were used for attaining the densification of TiB_2 with better mechanical properties [1–9]. As regards the fabrication routes, it has been noted that hot pressing and pressure-less sintering with the limited effort of using spark plasma sintering and microwave sintering are employed to densify TiB_2 [1,10]. Despite significant efforts in material development, bulk TiB_2 materials have not yet penetrated into commercial market in a big way. The bottleneck for such limitation is the processing difficulties, poor mechanical properties in terms of fracture toughness and moderate oxidation resistance [1,11].

* Corresponding author.
E-mail address: murthi@barc.gov.in (T.S.R.Ch. Murthy).

http://dx.doi.org/10.1016/j.jallcom.2016.01.216
0925-8388/

Table 1
Mechanical and physical properties of TiB_2 [1,5] and EuB_6 [15,17].

Property	TiB_2	EuB_6
Crystal structure	Hexagonal	Cubic
Density g/cc	4.52	4.99
Melting point °C	3225	2580
Hardness, GPa	25–35	26.1
Fracture toughness, MPa·$m^{1/2}$	5–7	3.2
Elastic modulus GPa	560	–
Flexural strength	700–1000	183
Coefficient of thermal expansion x 10^6/K	7.3	6.9
Thermal conductivity W/m/K	60–120	23
Electrical resistivity, μΩ·cm	10–40	–
Oxidation resistance °C	1100	–

Table 2
Details of starting powders of TiB_2 [3] and EuB_6 [17].

Property/composition	TiB_2	EuB_6
Mean particle diameter, μm	1.1	1.5
Specific surface area, m^2/g	7.12	–
carbon, wt%	0.6	0.7
Oxygen, wt%	0.5	0.6
Nitrogen, wt%	0.5	–
Phases identified by XRD	TiB_2	EuB_6

One of the promising applications of TiB_2 includes high temperature structural materials. It can be noted that TiB_2 could be an excellent choice for applications requiring heat dissipation at high temperatures due to its high thermal conductivity [1,12]. The oxidation resistance of TiB_2 is affected by temperature, partial pressure of oxygen, time of exposure, porosity and sintering additives. It is reported that oxidation resistance of TiB_2+silicide based composite could be improved by forming a in-situ protective amorphous fluid borosilicate coatings on the external surfaces directly facing the oxidizing environment at high temperature [1,8,12,13]. Addition of rare-earth elements could be useful approach to improve the oxidation resistance of borides at intermediate temperatures in hypersonic air. Addition of LaB_6 to ZrB_2 improved the oxidation resistance by formation of a $La_2Zr_2O_7$ [14]. EuB_6 addition also improved the oxidation resistance of ZrB_2 at the temperature of 900 °C by the formation of protective layer [15]. Addition of La_2O_3 to HfB_2, altered the oxidation kinetics [16].

This paper presents the study on the effect of EuB_6 on densification, microstructure and oxidation behavior of TiB_2. EuB_6 has high melting point, low thermal expansion coefficient, good thermal conductivity, high hardness, high wear resistance and chemical stability. It would be a suitable additive to TiB_2 for high temperature applications [17]. EuB_6 is an excellent neutron absorber material due to high neutron absorption cross section of both boron and europium [15,17,18]. Neutron absorption cross section of boron and europium are 759 and 4600 b respectively, which is quite a higher value [15,17,19]. It is considered a candidate material for control rod application in fast reactors [15,17,20]. The structure of the EuB_6 is quite loose with considerable room to accommodate helium atoms (which generated during neutron absorption) and thus it is

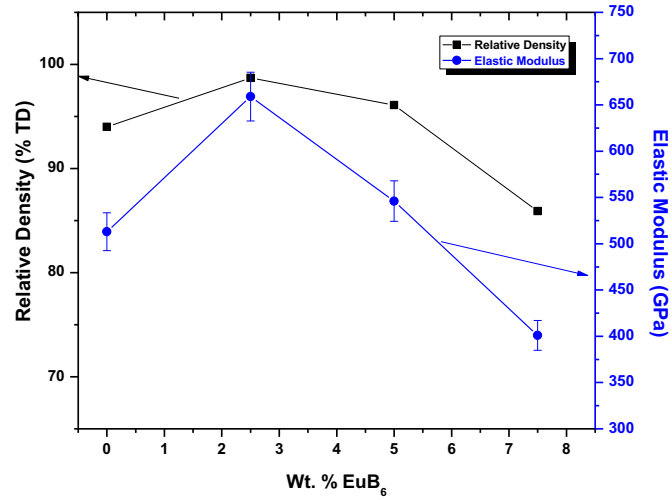

Fig. 1. Effect of EuB_6 addition on relative density and elastic modulus of TiB_2- hot pressed at 1750° C, 1h, 35 MPa.

resistant to irradiation swelling [15,18,20]. Crystal structure of EuB_6 is cubic (CsCl type) in which B_6 octahedra occupies corner sites and Eu occupies body centered site [21]. EuB_6 has also been reported to have resistance to oxidation which is due to the formation of Eu_2O_3 based protective layer [15]. Important properties of TiB_2 and EuB_6 are presented in Table 1 [1,5,15,17]. As per authors knowledge there is no literature report on the use of EuB_6 as sinter additive to TiB_2.

2. Experimental

2.1. Starting material

In house prepared TiB_2 (D_{50}: 1.1 μm, Sp.Surface area-7.12 m^2/g, 'C': 0.6 wt.%, 'O':0.5 wt.%, 'N':0.5 wt.%) and EuB_6 (D_{50}: 1.5 μm, 'C': 0.7 wt.%, 'O':0.6 wt.%) powders were used as starting materials. Starting materials (TiB_2 & EuB_6) were prepared by carbothermic reduction of its oxides in the presence of boron carbide. More details on synthesis of TiB_2 and EuB_6 powder are presented elsewhere [3,17]. Mean particle diameters of starting powders were measured by laser diffraction method (CILAS PSA 1064L). Table 2 presents the details of starting powders.

2.2. Densification and characterization

For densification, weighed quantities of fine titanium diboride and europium hexaboride were mixed thoroughly using a motorized mortar and pestle in dry condition for 1h to obtain samples of different compositions. The powder mixtures of TiB_2 +0% EuB_6, TiB_2 +2.5wt.% EuB_6, TiB_2 +5wt.% EuB_6 and TiB_2 +7.5wt.% EuB_6 were loaded in a high density graphite die (17 mm dia cavity) and hot pressed at a temperature of 1750 °C under a pressure of 35 MPa for 1 h in a high vacuum (0.001 Pa) chamber. The pellets were ejected from the die after cooling and the density measured by Archimedes' method in deionized water. Dimensions of densified

Table 3
Relative density, Hardness, Fracture toughness and Elastic modulus of TiB_2+EuB_6 ceramic based materials (hot pressed at 1750° C, 1h, 35 MPa).

EuB_6 (%wt.)	Actual density (g/cc)	Relative density (%TD)	Micro hardness (GPa)	Fracture toughness K_{IC} (MPa·$m^{1/2}$)	Elastic modulus (GPa)
0	4.25	94.1	27 ± 1	3.5 ± 0.1	513 ± 21
2.5	4.47	98.7	24 ± 1	5.2 ± 0.2	659 ± 26
5.0	4.36	96.1	26 ± 1	4.7 ± 0.1	546 ± 22
7.5	3.91	85.9	24 ± 1	4.0 ± 0.1	401 ± 16

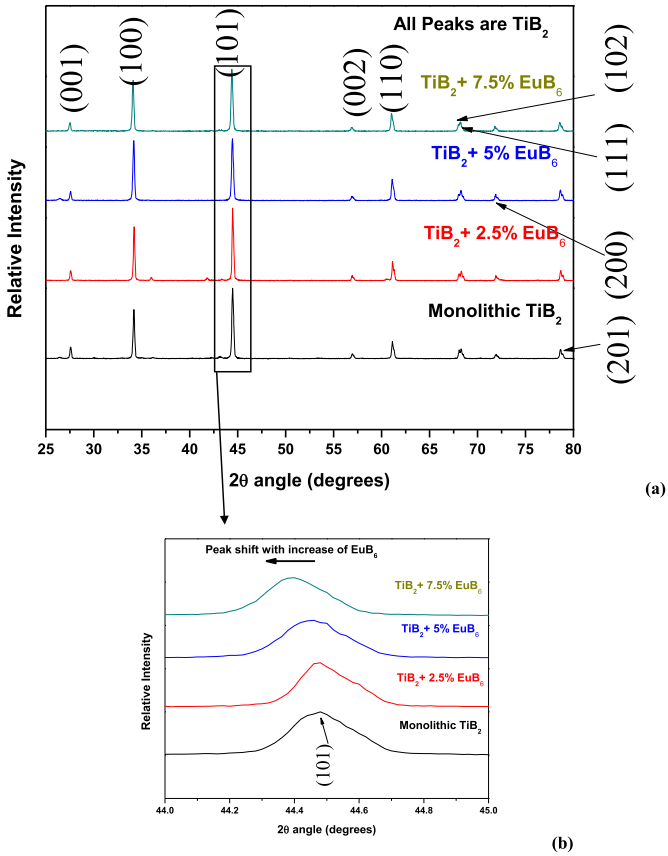

Fig. 2. a) XRD plots of hot pressed monolithic TiB_2 and $TiB_2 + EuB_6$ samples (Shows all peaks are TiB_2 only) - hot pressed at 1750° C, 1h, 35 MPa, b) zoomed portion of (101) peak indicates the shift in 2ɵ position with increase of EuB_6 addition in TiB_2.

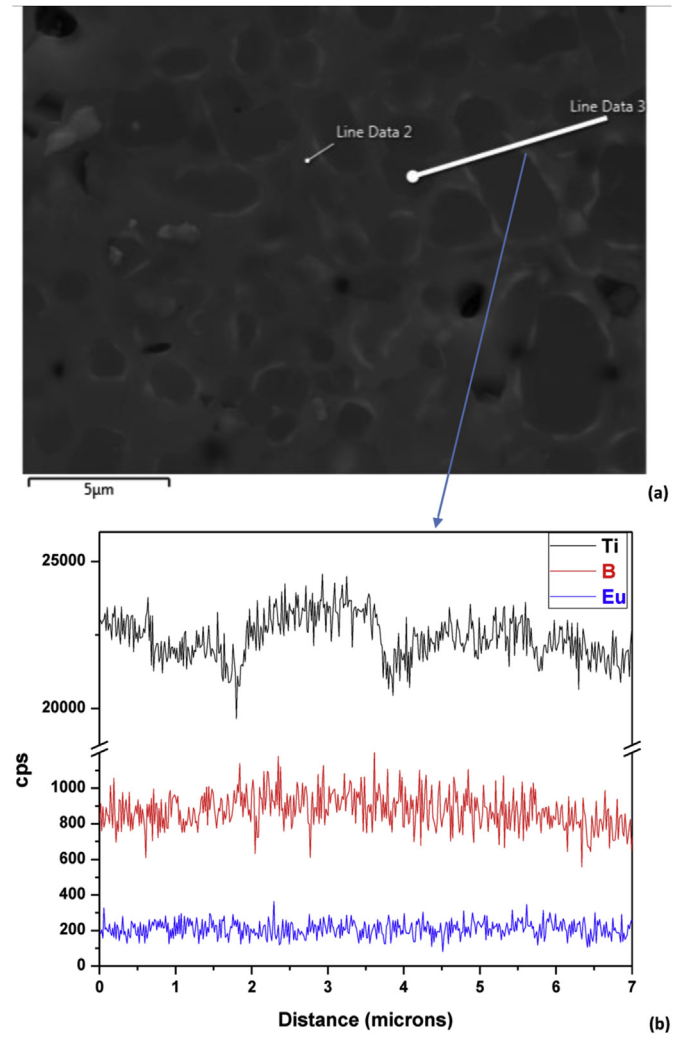

Fig. 3. Line scan across different grains of $TiB_2 + 5\%EuB_6$ sample for Ti, B and Eu a) SEM image, b) plot of number of counts vs. distance.

pellets are 17 mm diameter and ~6 mm thickness. Relative density (RD) was calculated by determining the volume fraction of porosity of the samples using image analysis technique on SEM images of the fractured samples. The reported density results are an average of 5 measurements that are performed on SEM micrographs of each sample by using Leica materials workstation version 3.6.6 software.

Densified samples were polished to mirror finish using diamond powder of various grades from 15 to 0.25 μm in an auto polisher (LaboForce-3, Struers). Micro hardness was measured on the polished surface at a load of 100 g and dwell time of 10 s. The indentation fracture toughness (K_{IC}) data were evaluated by crack length measurement of the crack pattern formed around Vickers indents (using 10 kg load), adopting the model formulation proposed by Anstis et al. [22], $K_{IC} = 0.016 \times (E/H)^{1/2}$ x $P/c^{3/2}$, where E is the Young's modulus, H-Vickers's hardness, P – applied indentation load, and c – half crack length. Young's modulus (E) of the all samples was measured by using ultrasonic pulse echo technique (UT 340, UTEX Scientific Instrument Inc., Canada). 15 MHz normal beam ultrasonic probe with a sampling rate of 1000 MHz was employed for velocity measurements. The reported value of hardness fracture toughness and Young's modulus is the average of five measured values. Polished samples were characterized by X-ray diffraction (XRD) using PHILIPS PW1830 X-ray diffractometer with Ni filtered Cu-Kα radiation for phase identification. Microstructural characterization of the polished and fractured samples were carried out by field emission scanning electron microscopy, energy dispersive spectroscopy (FESEM-EDS) and Electron back scattered diffraction (EBSD) using Carl Zeiss FESEM.

2.3. Oxidation

Isothermal oxidation studies for monolithic TiB_2 and TiB_2+EuB_6 sample were conducted at a temperature of 1400 °C in air up to 8h. Hot pressed pellet of diameter 17 mm was cut into thin slice of 2 mm thickness. All the surfaces of the cut sample were polished with emery papers (1/0, 2/0, 3/0, 4/0) and finally with diamond paste up to 1 μm finish. Oxidation tests were conducted in a resistance heated furnace. In order to avoid oxidation during heating, the sample was directly inserted into the furnace after the furnace temperature reached the required temperature. Samples were placed in an alumina crucible kept into the furnace. Each sample was carefully weighed before and after exposure to determine the weight changes during oxidation. Oxide phases formed on the surface were identified by XRD. The morphology and nature of oxide layer was examined by FESEM-EDS. TGA analysis of monolithic TiB_2 and TiB_2+EuB_6 sample were carried out up to 1200 °C in air with 10 K/min heating rate (NETZSCH STA 409 PC/PG) for continuous oxidation studies. Usually oxidized cross section samples are prepared by cutting the oxidized samples using abrasive diamond cutters, but success rate is very poor due to poor adherence of oxide layers. Special samples were prepared to study the cross section of oxidized specimens of monolithic TiB_2 and

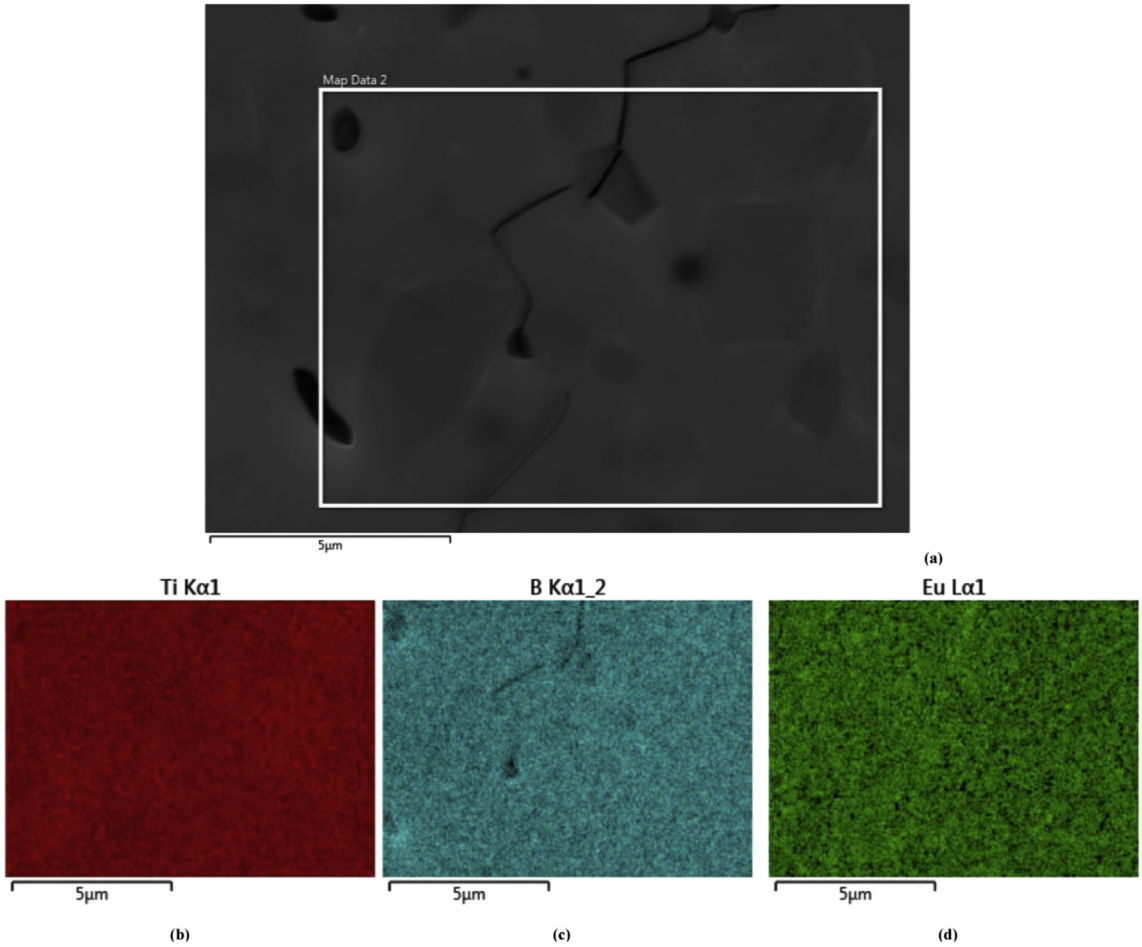

Fig. 4. Elemental mapping of TiB_2 + 5%EuB_6 sample for Ti, B and Eu a) SEM image, b) Ti, c) B, d) Eu.

TiB_2+EuB_6 sample in the present study. 3 mm dia hole was provided by using wire cut EDM, before oxidizing the sample. After oxidation, sample was polished in order to remove the outer oxide layer on the sample surface. Oxide cross section was obtained at the interface of hole and sample. The reported value of oxide thickness is the average of five measured values at different locations of image of cross section of isothermal oxidized samples.

3. Results

3.1. Densification and characterization

Hot pressing conditions, actual density and relative densities of the TiB_2 and TiB_2+EuB_6 samples are presented in Table 3. Fig. 1 presents the effect of EuB_6 addition on densification of TiB_2. Addition of 2.5wt.% EuB_6 resulted in densification of 98.7% TD at a temperature of 1750 °C and a pressure of 35 MPa. Samples with 5% EuB_6 were hot pressed up to 96.1%TD at similar processing conditions. A lower density of 85.9%TD was achieved in TiB_2+7.5% EuB_6 sample. In case of monolithic TiB_2, 97.5% TD density was obtained at a higher hot pressing temperature of 1800 °C [5]. In the present study, the hot pressing temperature was lower by 50 °C. Addition of EuB_6 toTiB_2 may result the formation of solid solution of TiB_2 and EuB_6. Formation of solid solution was confirmed by XRD and EBSD analysis of densified pellets, which is discussed in the next paragraphs.

XRD pattern of the dense pellet of monolithic TiB_2 and TiB_2+EuB_6 samples are shown in Fig. 2. It indicates the presence of crystalline TiB_2 peaks in all samples. Slight shift in the peaks were observed, with increasing the EuB_6 content more shift towards lower 2θ angle were observed. The major peak position of monolithic TiB_2 is at 44.48°, where as for TiB_2+5%EuB_6 and TiB_2+7.5% EuB_6 samples positions are at 44.46° and 44.40° respectively. Absence of EuB_6 and shift in the TiB_2 peaks in XRD patterns of sample indicates that the TiB_2 and EuB_6 form the complete solid solution.

Fig. 3 presents the BSE image of TiB_2+5% EuB_6. It shows the presence of different grains of same contrast. In line scan across different grains shows the presence of more or less uniform distribution of Ti, Eu and B elements. In order to ensure further, elemental mapping was taken over a region of the TiB_2+5% EuB_6 sample and presented in Fig. 4. Ti, B and Eu were uniformly presented all over the region. FESEM-EDS results reconfirm the XRD results, i.e. the formation of solid solution of TiB_2 and EuB_6.

In order to further confirm the presence of single phase in the sample EBSD analysis was carried out on specially polished TiB_2+5% EuB_6 sample. Figs. 5 and 6 present the EBSD images along with analyzed results. Fig. 5a) presents the image showing with different grains and b) grain size distribution plot. Mean grain diameter was calculated as 2.29 μm. Image (Fig. 5a) clearly shows the distribution of different sized equi-axed grains in the range of 1 μm–5 μm. These results indicates that, slight particle coarsening was observed in the hot pressed TiB_2+EuB_6 sample, as starting particle size are in the range of 1–1.5 μm particle coarsening could

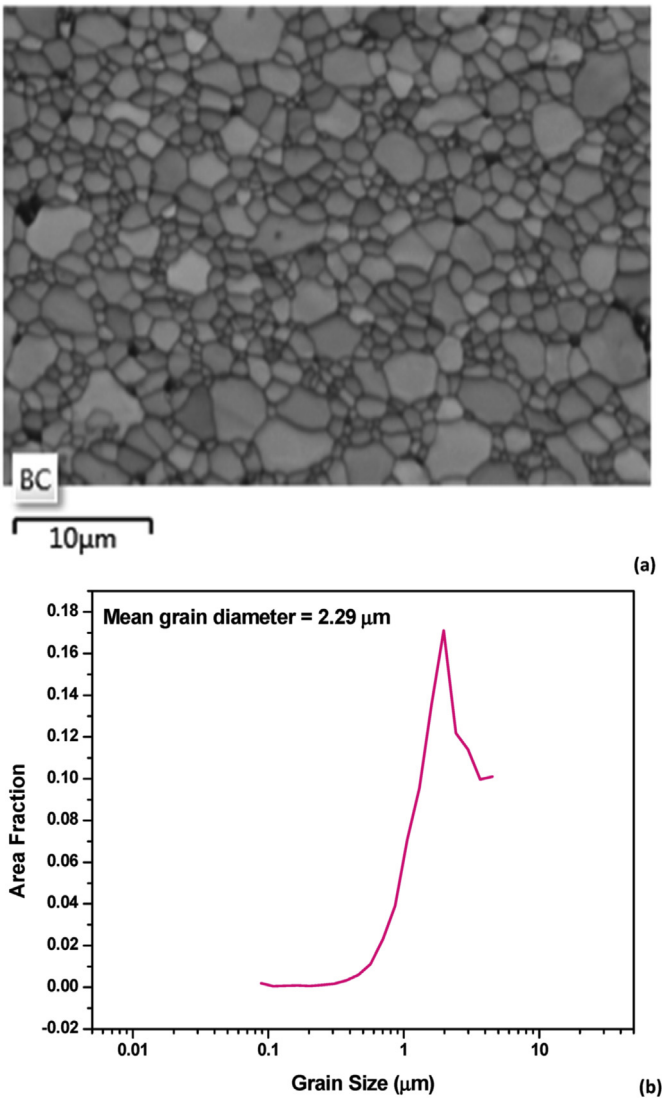

Fig. 5. a) Image showing the different sized grains and b) grain size distribution plot of TiB_2 + 5%EuB_6 sample.

be happened, while the formation of solid solution. Fig. 6a) present the orientation of different grains in the TiB_2+5% EuB_6 sample with different color coding. This image indicates that there is no preferential texture in the microstructure. Fig. 6b) present the EBSD image with different phases in different color coding along with quantification data of phases in tabular format. Entire image shows the presence of TiB_2 phase (blue (in the web version) color) only and hardly any EuB_6 phase (red (in the web version) color). This observation confirms the XRD results, i.e. the formation of solid solution of TiB_2 and EuB_6. For colors, please refer to the online version of the article. However, about 12% zero solutions are recorded in the sample, this could be due to polish pullouts and original porosity (~4%) in the sample. Polish pullouts are inevitable in ceramic samples, while doing the mirror finish polishing.

3.2. Mechanical properties and fractography

Variation in micro hardness, fracture toughness and elastic modulus of monolithic TiB_2 and TiB_2+EuB_6 samples are presented in Table 3. Effect of EuB_6 addition on mechanical properties is presented in Figs. 1 and 7. Hardness of all samples are in the range of 24–27 GPa. Variation of hardness is not so significant. The hardness value of TiB_2+7.5% EuB_6 sample is remained as 24 GPa, even it is having the low density of 86%TD only. It could be due to the solid solution hardening by formation of TiB_2+EuB_6 solid solution. On formation of solid solution the parent lattice gets strained (confirmed by XRD) and results in hardening of material. Fig. 8 presents the fracture surfaces of monolithic TiB_2 and TiB_2+5% EuB_6 sample. The mode of fracture is seen to be intergranular in both samples. Regular faceted grains are clearly visible. Grains were observed slightly bigger in the TiB_2+EuB_6 sample compared with monolithic.

Fracture toughness of monolithic TiB_2 and TiB_2+EuB_6 samples are presented in Fig. 7. Fracture toughness of monolithic TiB_2 sample was measured as 3.5 MPa $m^{1/2}$. ~50% higher fracture toughness value of 5.2 MPa $m^{1/2}$ was obtained for TiB_2+2.5% EuB_6 sample. For TiB_2+5% EuB_6, TiB_2+7.5% EuB_6 the fracture toughness values are 4.7 MPa $m^{1/2}$ and 4.0 MPa $m^{1/2}$ respectively. The fracture toughness values obtained in the TiB_2+EuB_6 sample samples are higher than the monolithic TiB_2. However, slightly lower fracture toughness values are recorded for 5% and 7.5% EuB_6 samples, compared with 2.5% EuB_6 sample. This could be due to the decrease in relative density. Fig. 9 presents the features of indentation crack in monolithic TiB_2 and TiB_2+5%EuB_6 sample samples. Slight crack deflections are mainly observed in monolithic TiB_2, where as both crack deflections and bridging mechanisms are observed in the TiB_2+EuB_6 sample, which explain the good fracture toughness.

3.3. Oxidation study

The weight gain data obtained during continuous oxidation of monolithic TiB_2 and TiB_2+5%EuB_6 samples are presented in Fig. 10. Weight gain started for monolithic TiB_2 at ~700 °C, whereas for TiB_2+EuB_6 sample at ~500 °C. Rate of weight gain for TiB_2+EuB_6 sample is very high upto ~600 °C, afterwards weight gain rate decreased upto 800 °C. Above 800 °C, both samples show the similar rate of weight gain upto 1200 °C. EuB_6 has more affinity for oxygen and hence oxidation started early (~500 °C) and also resulted in higher weight gain.

Isothermal oxidation studies were carried out at 1400 °C for monolithic TiB_2 and TiB_2+5%EuB_6 samples. Specific weight gain after 4h are recorded as 0.244 kg/m^2 and 0.479 kg/m^2 respectively for monolithic TiB_2 and TiB_2+5%EuB_6 sample. After 8h of oxidation at 1400 °C, specific weight gain was calculated as 0.505 kg/m^2 and 0.410 kg/m^2 respectively. After 1200 °C, it is expected that evaporation of sub oxides of boron. As, the both samples are having the substantial boron content, it is not worth to calculate the specific weight gain data. Hence, further oxidation kinetics was not evaluated. However, oxidized surfaces were examined by XRD and FESEM-EDS. Fig. 11 presents the XRD pattern of oxidized surfaces of monolithic TiB_2 and TiB_2+EuB_6 samples at 1400 °C for 8h. Only TiO_2 peaks were observed on the oxidized surface of monolithic TiB_2. As expected, all B_2O_3 or sub oxides of boron are evaporated from the surface at 1400 °C. On other hand, $EuBO_3$ and Eu_2O_3 peaks were identified in addition to TiO_2 on the oxidized surface of TiB_2+5% EuB_6 sample. SEM image of oxidized surface along with elemental mapping and EDS spot analysis are presented in Figs. 12 and 13 for monolithic TiB_2 and TiB_2+EuB_6 sample respectively. Oxidized surface of monolithic TiB_2 (Fig. 12) image clearly shows the presence of highly textured TiO_2 dendrites (marked on the image) and whole surface is not evenly covered. Some holes (marked on the image) were observed on the oxidized surface, it may be resulted from the evaporation of sub oxides of boron. Elemental mapping of the region shows presence of rich in Ti and O some traces of B. Spot analysis was carried out on dendrites and glassy phase region (Fig. 12). Dendrites were confirmed as TiO_2. Oxidized surface of

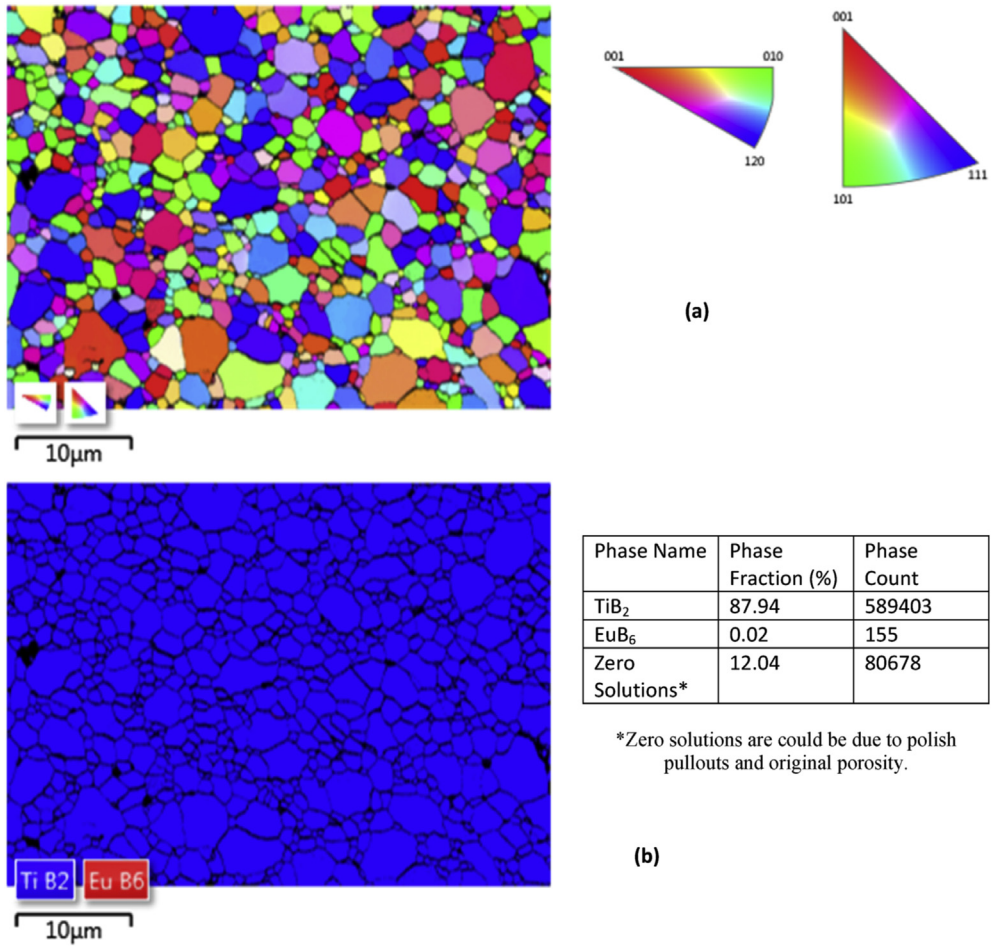

Phase Name	Phase Fraction (%)	Phase Count
TiB_2	87.94	589403
EuB_6	0.02	155
Zero Solutions*	12.04	80678

*Zero solutions are could be due to polish pullouts and original porosity.

Fig. 6. EBSD analysis of TiB_2 + 5%EuB_6 sample a) different orientation of grains with different color coding, b) color mapping of different phases of TiB_2 and EuB_6, quantitative data given in table. For colors, please refer to the online version of the article

TiB_2+EuB_6 sample image shows the more continuous oxide layer consisting of Ti, O, Eu and B (Fig. 13).

FESEM image of cross section of isothermal oxidized (1400 °C, 8h) samples of monolithic TiB_2 and TiB_2 + 5%EuB_6 sample are presented in Fig. 14 and Fig. 15 respectively. Total oxide cross section of monolithic TiB_2 was measured as 520 μm, where as for TiB_2 + 5%EuB_6 sample is only of 340 μm. Overview of the entire cross section of oxidized sample shows that more uniform width of the oxide layer was observed over the entire region for both samples. At higher magnifications, oxide layer of monoltich TiB_2 (Fig. 14) looks like loosely packed with some porosity. Whereas for TiB_2 + 5%EuB_6 sample, oxide layer is completely covered the entire region without any porosity (Fig. 15), which indicates that formed oxide layer is not allowing to ingress the oxygen through it. This data infers that addition of EuB_6 to TiB_2, helped to improve the oxidation resistance.

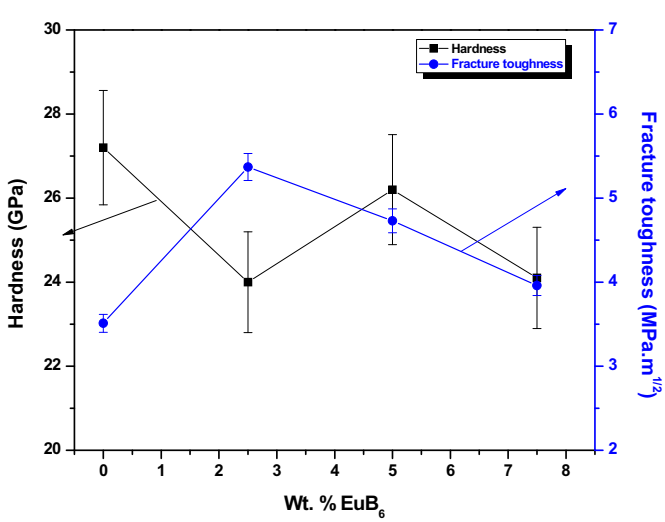

Fig. 7. Effect of EuB_6 addition on hardness and fracture toughness of TiB_2- hot pressed at 1750° C, 1h, 35 MPa.

4. Discussion

Owing to its strong covalent bonding and low self-diffusion coefficient, monolithic TiB_2 ceramic is always hard to achieve full densification and reported to be densified at or above 2000 °C [1,23,24]. The introduction of appropriate second phase particle is proved to be an efficient method to improve the sinterability. Wettability and dissolution of TiB_2 in the transient liquid phase have been widely identified as critical factors when sintering with metallic additives [1,23]. From the perspective of high temperature applications, the presence of metallic binder is not desirable: the low melting point of either sintering liquid or metallic additives leads to incipient fusion and consequent degradation of high

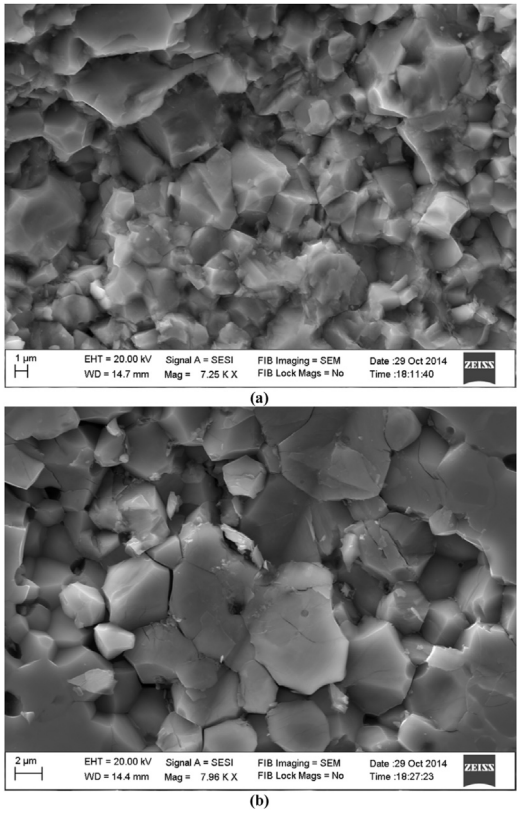

Fig. 8. Fractography of monolithic TiB_2 (a) and TiB_2 + 5%EuB_6 sample (b) (Shows intergranular mode of fracture).

temperature properties [1]. Various non-metallic additives (especially ceramic based) have been used for attaining densification of TiB_2 with retention of high temperature properties [1]. Especially 'Si' contained additives like silicon nitride, transition metal silicides are proved to be effective sinter additives in order to reduce the sintering temperature by liquid phase sintering and/or activated

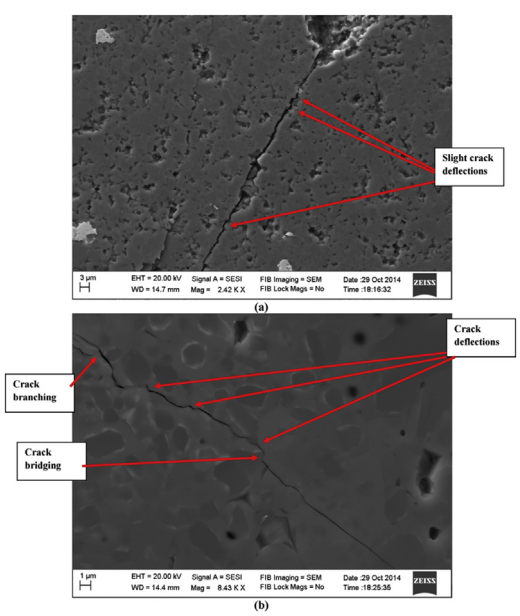

Fig. 9. Crack propagation pattern of a) monolithic TiB_2 and b) TiB_2 + 5%EuB_6 sample.

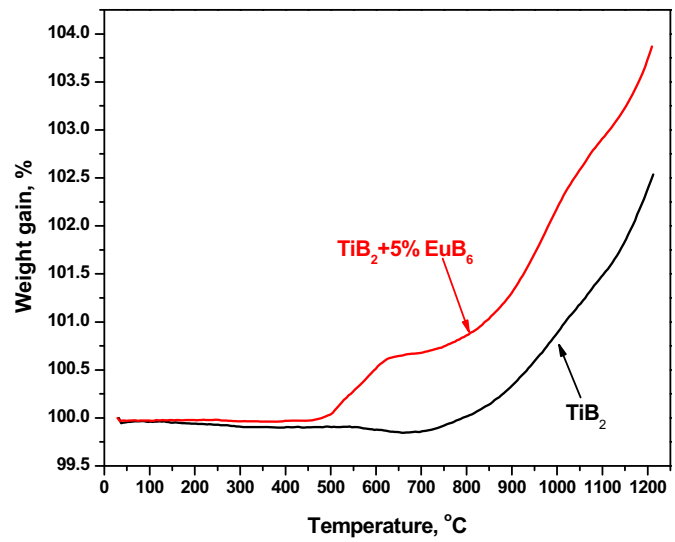

Fig. 10. Weight gain data of continuous oxidation in TGA for monolithic TiB_2 and TiB_2 + 5%EuB_6 sample in air up to 1200 °C at heating rate of 10 K/min.

sintering [1,8,11,12]. When CrB_2 is added to TiB_2, improvement in densification was seen due to the higher mobility of CrB_2 and formation of solid solution with TiB_2 [7]. Sonber et al. reported the improvement in densification of ZrB_2, when used the EuB_6 as additive by formation of solid solution [15]. Similar observations were also made in the present study that addition of 2.5% EuB_6 helped in densification by forming a solid solution with TiB_2. This is a complete solid state sintering, hence further addition of (beyond 5%) EuB_6 has not helped much to improve the densification. However, complete solid solution formation was confirmed in all the TiB_2+EuB_6 samples by XRD, EDS and EBSD.

Usually addition of second phase (sinter additive) will enhance the fracture toughness due to the compressive stresses at the interface of matrix and second phase. Origin for compressive stresses is due to the difference in coefficient of thermal expansion.

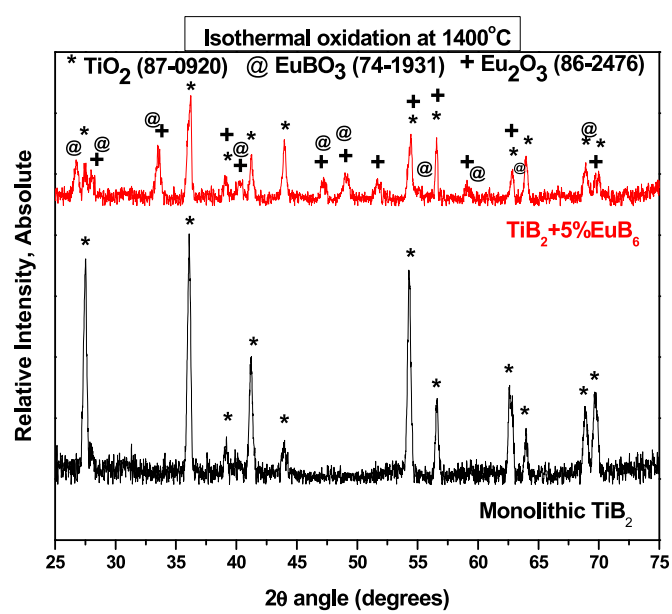

Fig. 11. XRD data of isothermal oxidized surfaces of monolithic TiB_2 and TiB_2 + 5%EuB_6 samples at 1400 °C, 8h.

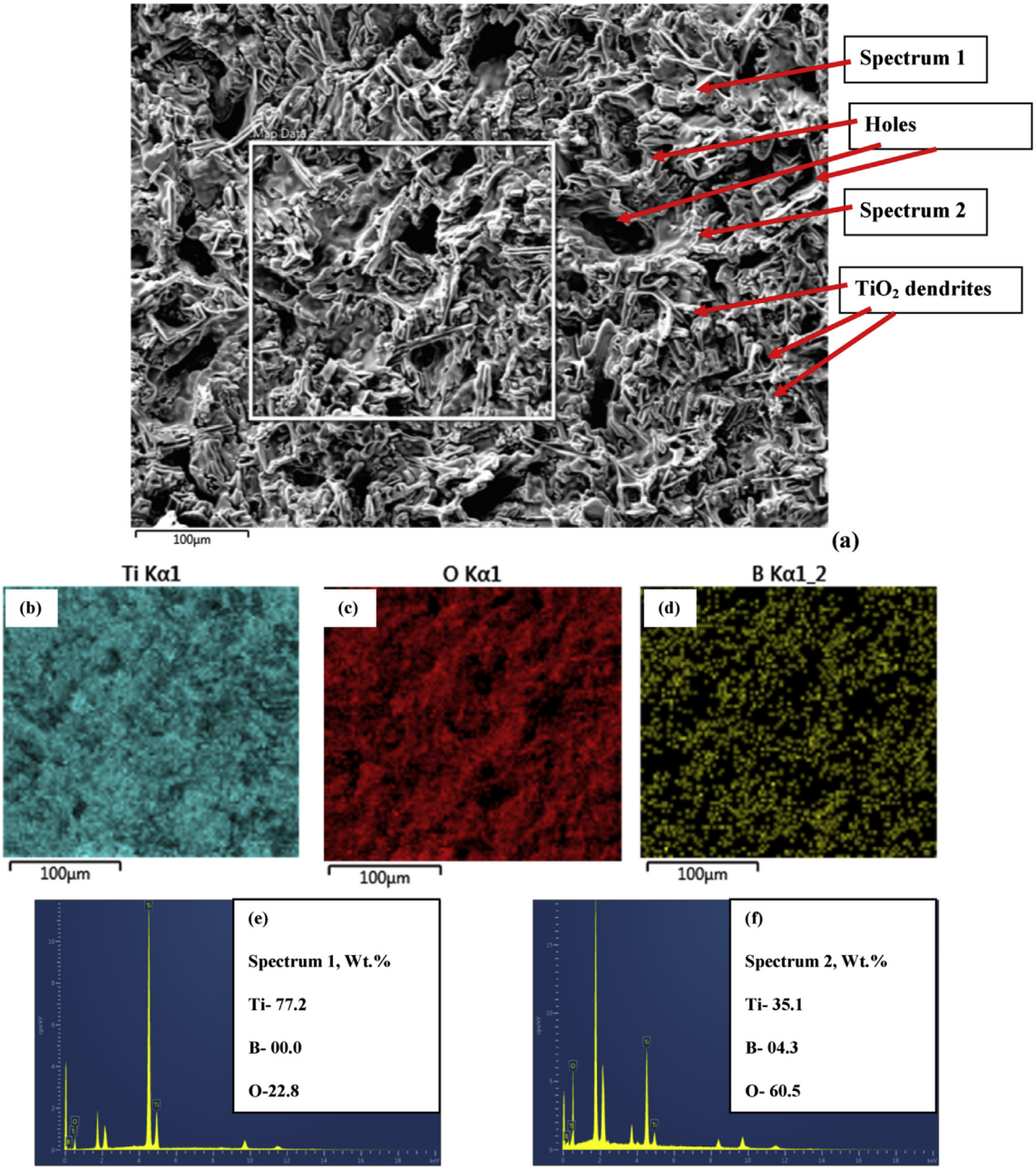

Fig. 12. a) FESEM image, Elemental mapping (b-Ti, c-O, d-B) and spot analysis (e-spectrum 1, f-spectrum 2) of isothermal oxidized surfaces of monolithic TiB2 sample at 1400 °C, 8h.

In some reports, observed the crack deflections, branching and bridging mechanisms due to the presence of second phases. Usually, in ceramics above cited mechanisms are responsible for the improvement of fracture toughness. Fracture toughness of monolithic TiB_2 was report in the range of 3–4 MPa $m^{1/2}$ [1]. By using non-metallic additives, slightly improved fracture toughness of ~6 MPa $m^{1/2}$ was reported [1]. As expected, further improvement of fracture toughness up to 10 MPa $m^{1/2}$ was reported by adding metallic additives due to plastic deformation of second phase [1]. ~50% higher fracture toughness value of 5.2 MPa $m^{1/2}$ was obtained in the present study by adding 2.5% EuB_6 to TiB_2. Crack deflection, branching and bridging mechanisms were mainly responsible for the improved fracture toughness value of the TiB_2 + 5%EuB_6 samples. The improvement of fracture toughness is could be due to the increase of density and therefore Young's modulus.

The oxidation of TiB_2 composites can be minimized either by providing resistance to the diffusion of oxygen ion into the material or to the diffusion of the base ceramic forming element ions through the oxide to the oxide-air interface. It is interesting to note that oxidation resistance of composite is not only depends on the type of sinter additive but also on the presence of quantity. In our earlier studies, found that with increasing sinter additive (transition silicides) content from 2.5 to 5 or 10%, nature of oxidation changes from linear to parabolic or cubic [6–10] up to 1000 °C. Boron/silicon based protective oxide layers (borosilicate/glassy phases) are only stable up to 1200 °C [1,6–10]. Beyond this temperature, additives based on rare earth elements such as La, Eu, Ce are attributed to improve the oxidation resistance of ultrahigh temperature ceramics (ZrB_2, HfB_2) [14–16] by forming a oxide products such as $La_2Zr_2O_7$, $LaBO_3$, Eu_2O_3 [14–16]. In the present

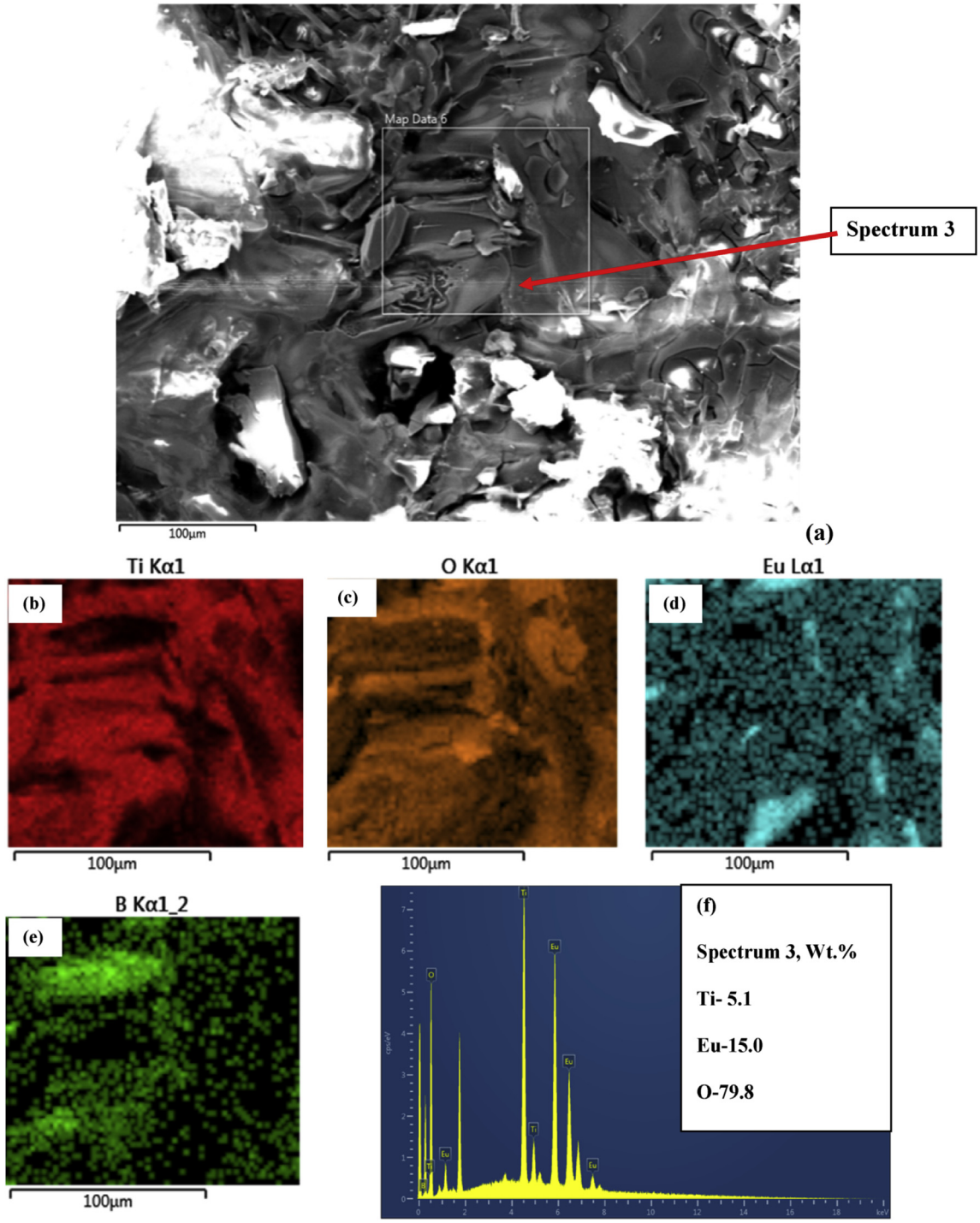

Fig. 13. a) FESEM image, Elemental mapping (b-Ti, c-O, d-Eu, e-B) and spot analysis (f-spectrum 3) of isothermal oxidized surfaces of TiB2 + 5%EuB6 sample at 1400 °C, 8h.

preliminary oxidation study also identified the oxide products of $EuBO_3$ and Eu_2O_3 after oxidation at 1400 °C for 8h. These oxide layers appear to be continuous and crack free.

The hypothesis behind the enhancement of oxidation resistance of TiB_2 by EuB_6 addition is presented in following lines. One possibility is the formation of very thin protective layer consisting of $EuBO_3$ and Eu_2O_3. EuB_6 has been reported to have good oxidation resistance which is due to the formation of Eu_2O_3 based protective layer [15]. Another possibility is the formation of protective layer by combined effect of Eu_2O_3 and TiO_2. TiO_2 layer alone is not protective and results in linear weight gain but Eu_2O_3 may be probably stabilizing the layer and making it protective by formation of solid solution between TiO_2 and Eu_2O_3. Following possible oxidation reactions are given below:

$$2/5TiB_2 + O_2 \rightarrow 2/5TiO_2 + 2/5B_2O_3 \quad (1)$$

$$4/21EuB_6 + O_2 \rightarrow 2/21Eu_2O_3 + 12/21B_2O_3 \quad (2)$$

$$2/21EuB_6 + O_2 \rightarrow 2/21\ EuBO_3 + 2/21B_2O_3 \quad (3)$$

As the thermodynamic data is not available for Eu–B system,

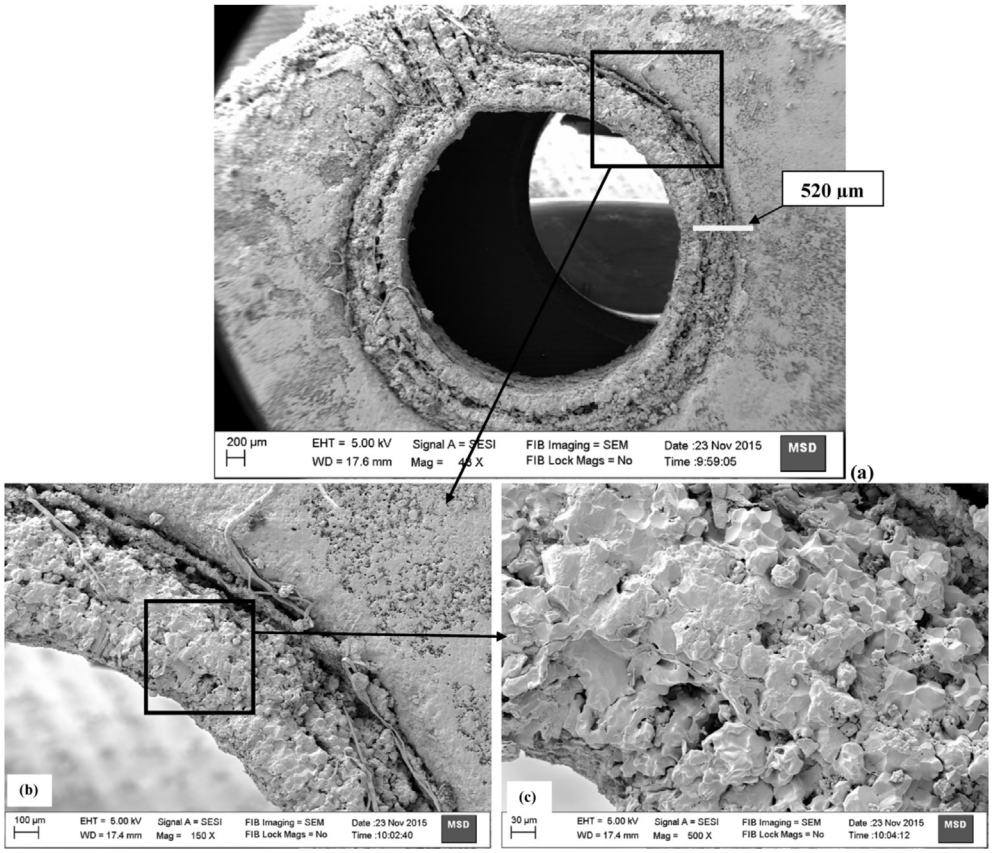

Fig. 14. a) FESEM image of cross section of isothermal oxidized sample of monolithic TiB2 sample at 1400 °C, 8h (Oxide layer thickness–520 µm) b) & c) are at higher magnification.

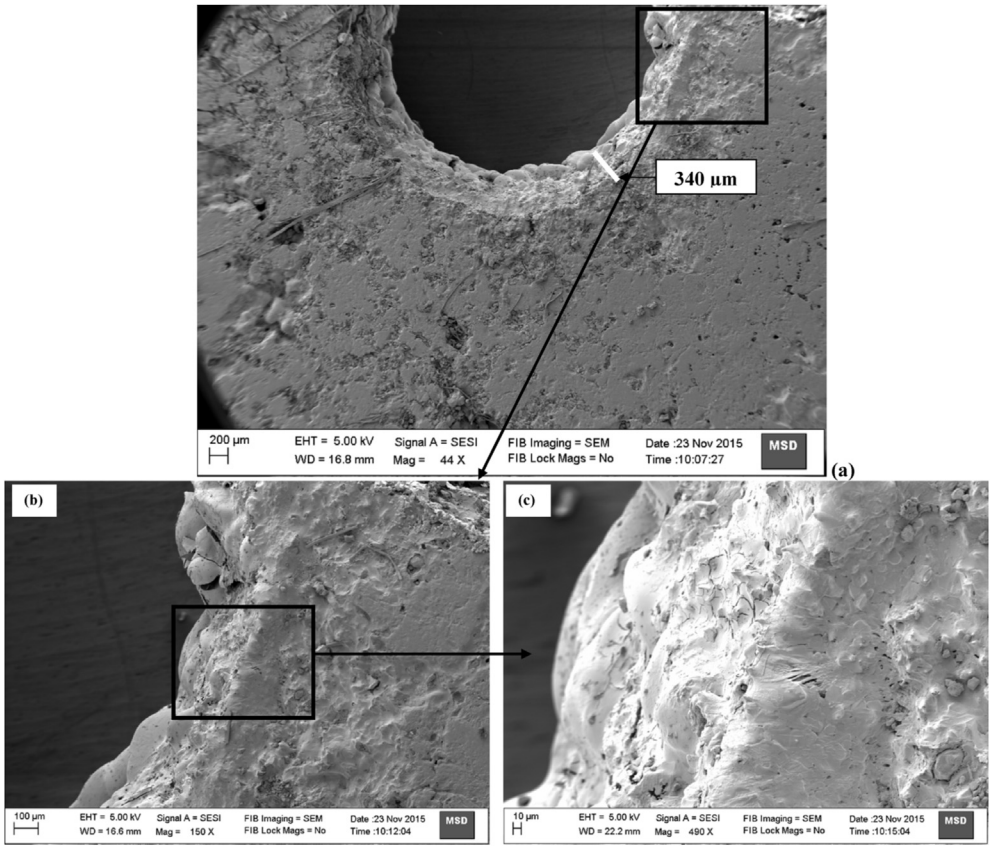

Fig. 15. a) FESEM image of cross section of isothermal oxidized sample of TiB2 + 5%EuB6 sample at 1400 °C, 8h (Oxide layer thickness–340 µm) b) & c) are at higher magnification.

could not calculate the free energy data for the formation of above reactions (2) & (3). Free energy data for the reaction (1) are reported elsewhere [9]. The weight gain of TiB_2+EuB_6 sample is more than that of TiB_2 (Fig. 10), but the overall oxide layer thickness is less in case of TiB_2+EuB_6 sample during isothermal oxidation at 1400 °C for 8h. EuB_6 has more affinity for oxygen than TiB_2, hence the higher weight gain was observed during continuous oxidation. But during isothermal oxidation at 1400 °C, for prolonged period of 8h resulted a formation of protective oxide layer in TiB_2+EuB_6 sample, which not allowed to further ingress of oxygen ions through it. As a result oxide layer thickness was ~35% less than that of monolithic TiB_2 observed in TiB_2+EuB_6 sample.

5. Conclusion

TiB_2+EuB_6 ceramic novel samples with different EuB_6 contents were fabricated using hot-pressing technique. The microstructure, mechanical properties and oxidation studies were carried out in detail. The following conclusions were drawn from the results:

(1) Addition of 2.5wt.%EuB_6 was found to be favoring the densification and resulting the maximum component density of ~98.7% TD.
(2) EuB_6 was observed to form a complete solid solution with TiB_2.
(3) Hardness of all samples is measured in the range of 24–27 GPa. Fractography indicate the mode of fracture is intergranular for TiB_2+EuB_6 sample.
(4) Maximum fracture toughness of 5.2 MPa $m^{1/2}$ was obtained, when 2.5wt.% EuB_6 was added with TiB_2.
(5) At 1400 °C, the oxide layer thickness of TiB_2+EuB_6 sample was measured as 340 μm, which is ~35% less than that of monolithic TiB_2 (520 μm). This enhancement in oxidation resistance was mainly due to the formation of $EuBO_3$ and Eu_2O_3 phases.

6. Acknowledgment

Authors would like to acknowledge contributions of Dr. Sanjay Kumar and Sri Uttam Jain for TGA of oxidation samples.

References

[1] B. Basu, G.B. Raju, A.K. Suri, Processing and properties of monolithic TiB_2 based materials, Int. Mater. Rev. 51 (6) (2006) 354–374.
[2] R.G. Munro, J. Res. Natl. Inst. Stand. Technol. 105 (5) (2000) 709–720.
[3] B. Huang, S. Chen, Z. Yao, M. Zhang, Y. Jing, B. Li, W. Xiong, Study of carbothermal synthesis of TiB_2 assisted by extended high-energy milling, Powder Technol. 275 (2015) 69–76.
[4] C. Subramanian, A.K. Suri, Development of boron based neutron absorber materials, Metals Mater. Process. 16 (1) (2004) 39–52.
[5] T.S.R.Ch. Murthy, B. Basu, R. Balasubramaniam, A.K. Suri, C. Subramanian, R.K. Fotedar, Processing and properties of TiB_2 with $MoSi_2$ sinter-additive: a first report, J. Am. Ceram. Soc. 89 (1) (2006) 131–138.
[6] G.B. Raju, B. Basu, N.H. Tak, S.J. Cho, Temperature dependent hardness and strength properties of TiB_2 with $TiSi_2$ sinter-aid, J. Eur. Ceram. Soc. 29 (10) (2009) 2119–2128.
[7] T.S.R.Ch. Murthy, J.K. Sonber, C. Subramanian, R.K. Fotedar, M.R. Gonal, A.K. Suri, Effect of CrB_2 addition on densification, properties and oxidation resistance of TiB_2, Int. J. Refract. Met. Hard Mater. 27 (6) (2009) 976–984.
[8] Z.H. Zhang, X.B. Shen, F.C. Wang, S.K. Lee, Q.B. Fan, M.S. Cao, Low-temperature densification of TiB_2 ceramic by the spark plasma sintering process with Ti as a sintering aid, Scr. Mater. 66 (3–4) (2012) 167–170.
[9] T.S.R.Ch. Murthy, J.K. Sonber, C. Subramanian, R.C. Hubli, A.K. Suri, Densification, characterization and oxidation studies of TiB_2 + WSi_2 composite, Int. J. Refract. Met. Hard Mater 33 (2012) 10–21.
[10] A. Turan, F.C. Sahin, G. Goller, O. Yucel, Spark plasma sintering of monolithic TiB_2 ceramics, J. Ceram. Process. Res. 15 (6) (2014) 464–468.
[11] G.B. Raju, K. Biswas, B. Basu, Microstructural characterization and isothermal oxidation behavior of hot-pressed TiB_2-10wt.% $TiSi_2$ composites, Scr. Mater. 61 (2009) 104–107.
[12] T.S.R.Ch. Murthy, J.K. Sonber, C. Subramanian, R.C. Hubli, N. Krishnamurthy, A.K. Suri, Densification and oxidation behavior of a novel $TiB_2 - MoSi_2 - CrB_2$ composite, Int. J. Refract. Met. Hard Mater. 36 (2013) 243–253.
[13] T.S.R.Ch. Murthy, J.K. Sonber, C. Subramanian, R.C. Hubli, N. Krishnamurthy, A.K. Suri, Densification, characterization and oxidation studies of (TiCr)B_2+20%$MoSi_2$, Int. J. Refract. Met. Hard Mater. 37 (2013) 12–28.
[14] F. Monteverde, D. Alfano, R. Savino, Effects of LaB_6 addition on arc-jet convectively heated SiC-containing ZrB_2-based ultra-high temperature ceramics in high enthalpy supersonic airflows, Corros. Sci. 75 (2013) 443–453.
[15] J.K. Sonber, T.S.R.Ch. Murthy, C. Subramanian, R.C. Hubli, A.K. Suri, Effect of EuB_6 addition on densification and properties of ZrB_2, Int. J. Refract. Met. Hard Mater. 35 (2012) 96–101.
[16] D.D. Jayaseelan, E.Z. Solvas, C.M. Camey, Z. Katz, P. Brown, W.E. Lee, Microstructure and evaluation of HfB_2 based ceramic during oxidation at 1600-2000°C, Adv. Appl. Ceram. 114 (5) (2015) 277–295.
[17] J.K. Sonber, T.S.R.Ch. Murthy, C. Subramanian, R.C. Hubli, A.K. Suri, Synthesis, densification and characterization of EuB_6, Int. J. Refract. Met. Hard Mater. 38 (2013) 67–72.
[18] T. Fujita, M. Suzuki, Y. Ishikawa, Specific heat of EuB_6, Solid State Commun. 33 (9) (1980) 947–950.
[19] F. Thevenot, A review on boron carbide, Key Eng. Mater. 56–57 (1991) 59–88.
[20] Z. Fisk, D.C. Johnston, B. Cornut, S.V. Molnar, S. Oseroff, Magnetic, transport, and thermal properties of ferromagnetic EuB_6, J. Appl. Phys. 50 (3) (1979) 1911–1913.
[21] B.G. Arabei, E.N. Shtrom, Y.A. Lapitskii, Characteristics of the manufacturing technology of dense parts from, and the mechanical properties of, some hexaborides of the rare-earth metals, Powder Metall. Met. Ceram. 3 (5) (1964) 406–409.
[22] G.R. Anstis, P. Chantikul, B.R. Lawn, D.B. Marshall, A critical evaluation of indentation techniques for measuring fracture toughness: i, direct crack measurements, J. Am. Ceram. Soc. 64 (1981) 533–538.
[23] V.I. Matkovich, Boron and Refractory Borides, Springler-Verlag, Berlin, Heidelberg, New York, 1977.
[24] D. Demirskyi, Y. Sakka, O. Vasylkiv, High-temperature reactive spark plasma consolidation of TiB_2–NbC, Ceram. Compos. Ceram. Int. 41 (2015) 10828–10834.